JACS
JOURNAL OF THE AMERICAN CHEMICAL SOCIETY

Article

pubs.acs.org/JACS

Versatile Photocatalytic Systems for H_2 Generation in Water Based on an Efficient DuBois-Type Nickel Catalyst

Manuela A. Gross,[†] Anna Reynal,*[,‡] James R. Durrant,[‡] and Erwin Reisner*[,†]

[†]Christian Doppler Laboratory for Sustainable SynGas Chemistry, Department of Chemistry, University of Cambridge, Lensfield Road, Cambridge CB2 1EW, U.K.

[‡]Department of Chemistry, Imperial College London, Exhibition Road, London SW7 2AZ, U.K.

Supporting Information

ABSTRACT: The generation of renewable H_2 through an efficient photochemical route requires photoinduced electron transfer (ET) from a light harvester to an efficient electrocatalyst in water. Here, we report on a molecular H_2 evolution catalyst (**NiP**) with a DuBois-type $[Ni(P_2^{R'}N_2^{R''})_2]^{2+}$ core ($P_2^{R'}N_2^{R''}$ = bis(1,5-R′-diphospha-3,7-R″-diazacyclooctane), which contains an outer coordination sphere with phosphonic acid groups. The latter functionality allows for good solubility in water and immobilization on metal oxide semiconductors. Electrochemical studies confirm that **NiP** is a highly active electrocatalyst in aqueous electrolyte solution (overpotential of approximately 200 mV at pH 4.5 with a Faradaic yield of 85 ± 4%). Photocatalytic experiments and investigations on the ET kinetics were carried out in combination with a phosphonated Ru(II) tris(bipyridine) dye (**RuP**) in homogeneous and heterogeneous environments. Time-resolved luminescence and transient absorption spectroscopy studies confirmed that directed ET from **RuP** to **NiP** occurs efficiently in all systems on the nano- to microsecond time scale, through three distinct routes: reductive quenching of **RuP** in solution or on the surface of ZrO_2 ("on particle" system) or oxidative quenching of **RuP** when the compounds were immobilized on TiO_2 ("through particle" system). Our studies show that **NiP** can be used in a purely aqueous solution and on a semiconductor surface with a high degree of versatility. A high TOF of 460 ± 60 h^{-1} with a TON of 723 ± 171 for photocatalytic H_2 generation with a molecular Ni catalyst in water and a photon-to-H_2 quantum yield of approximately 10% were achieved for the homogeneous system.

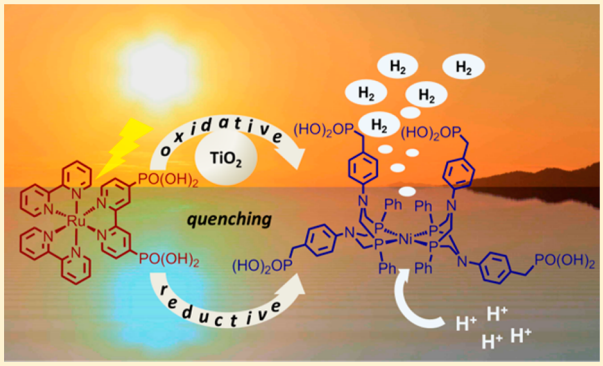

INTRODUCTION

The sunlight-driven generation of the energy carrier H_2 from water using earth-abundant materials is considered one of the key processes to generate more sustainable fuels in a postfossil age.[1] Synthetic first-row transition-metal complexes containing Co,[2] Fe,[3] and Ni[4] are under intense development as scalable alternatives to the benchmark H_2 evolution catalysts platinum[5] and hydrogenases.[6] Complexes with a catalytic bis(1,5-R′-diphospha-3,7-R″-diazacyclooctane)nickel(II) core, $[Ni(P_2^{R'}N_2^{R''})_2]^{2+}$, developed by DuBois and co-workers, emerged in the past decade as probably the most active synthetic 3d transition-metal electrocatalysts for proton reduction.[4b,c,7] The catalytic cycle has been studied experimentally[8] and computationally,[9] and the catalyst mimics important features of the hydrogenase active site.[4c,7c,10]

Photocatalytic H_2 generation requires the efficient coupling of an efficient proton reduction electrocatalyst with a light-harvesting component. In particular, the development and investigation of molecular H_2 evolution catalysts made of abundant elements that show stability and activity in water are of major interest.[11] Many reports on homogeneous photocatalytic systems for water reduction using Fe[3a,e,12] or Co[2b,13] complexes are available, but there are relatively few using Ni-based catalysts.[4f−i,14] Heterogenization of well-defined molecular catalysts on semiconductor surfaces is an emerging approach for photocatalytic H_2 generation. Systems that have been shown to have notable H_2 production efficiencies include cobaloximes immobilized on TiO_2 nanoparticles[13f−i] or CdSe/ZnS quantum dots,[13j] and [FeFe]-hydrogenase mimics on CdTe[12a] or ZnS[15] quantum dots. Efforts have also been made to integrate molecular catalysts on photoelectrodes, such as an [FeFe] complex on InP,[12c] a cobaloxime catalyst on p-type GaP,[16] and Fe(dithiolato)(diphosphine)[17] or cobaloxime catalysts[18] on dye-sensitized NiO films. However, the frequent use of organic solvents, poor light-to-H_2 conversion efficiencies, and photoinstabilities are drawbacks in these systems.

Despite the promising properties of DuBois-type catalysts, they were previously only applied in homogeneous photocatalytic schemes in the presence of organic solvents or a biological matrix.[4g,19] Surface immobilization of a $[Ni(P_2^{R'}N_2^{R''})_2]^{2+}$ derivative on carbon nanotubes yielded highly

Received: October 16, 2013
Published: December 9, 2013

   dx.doi.org/10.1021/ja410592d | J. Am. Chem. Soc. 2014, 136, 356−366

active electrodes for H_2 generation under strongly acidic conditions.[4e] When a $[Ni(P_2^{R'}N_2^{R''})_2]^{2+}$ derivative was immobilized on a p-type silicon photoelectrode, no (photo)-activity for H_2 production was reported.[20] Water-soluble $[Ni(P_2^{R'}N_2^{R''})_2]^{2+}$ derivatives were previously not shown to operate in aqueous homogeneous or heterogeneous environments for photocatalytic H_2 generation.

In this work, we report on a novel DuBois-type catalyst (**NiP**; Figure 1), which not only contains a highly electroactive

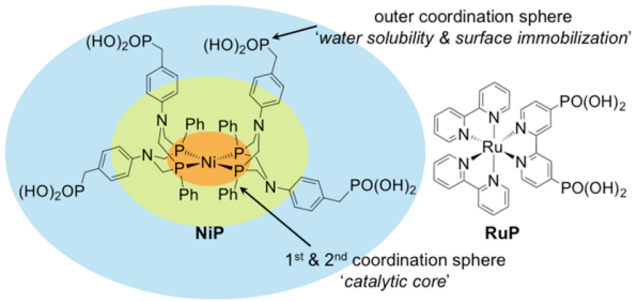

Figure 1. Chemical structures of the doubly charged cationic complexes used in this study: the electrocatalyst **NiP** and dye **RuP**. Both complexes have bromide counterions.

$[Ni(P_2^{R'}N_2^{R''})_2]^{2+}$ core, but also is surrounded by an outer sphere containing four dangling phosphonic acid moieties. This outer-sphere feature provides the catalyst with good solubility in aqueous solutions and anchors for immobilization onto metal oxide surfaces.[21] Electrochemical studies of **NiP** in an aqueous electrolyte solution demonstrated sustained electrocatalytic activity in the absence of organic solvents. Subsequently, we studied **NiP** in aqueous photochemical systems with a phosphonated bipyridine-based Ru(II) photosensitizer (**RuP**; Figure 1) in both a homogeneous system and heterogeneous photocatalytic environments where **RuP** and **NiP** were immobilized on different metal oxide semiconductors.

The kinetics of charge separation and recombination were studied by time-correlated single photon counting (TC-SPC) and transient absorbance spectroscopy (TAS). This spectroscopic study reveals that distinct reaction mechanisms are possible in these remarkably versatile photochemical systems. In particular, we consider whether this coimmobilization strategy on metal oxide surfaces reduces the rapid electron/hole recombination losses typically observed when such photosensitizers and catalysts are covalently attached via molecular linker groups.[22] The visible-light-driven H_2 generation of the different systems was also studied in bulk experiments and revealed that **NiP** can operate with a high photocatalytic turnover frequency for a Ni-based molecular proton reduction catalyst in purely aqueous systems.

EXPERIMENTAL SECTION

Materials and Methods. All synthetic procedures involving air- or moisture-sensitive materials were carried out under N_2 by using either a glovebox or Schlenk techniques. Chemicals for the synthetic part of this work were purchased from commercial suppliers and used without further purification. Solvents were dried using standard purification procedures under an N_2 atmosphere. Chemicals for analytical measurements were purchased in the highest available purity. TiO_2 nanoparticles (Aeroxide TiO_2 P25 particles; anatase/rutile (8/2) mixture, average particle size 21 nm) were a gift from Evonik Industries, and ZrO_2 nanoparticles (99.9%, 20−30 nm) were obtained from Skyspring Nanomaterials Inc. Nanostructured anatase TiO_2 and ZrO_2 films were prepared by the Doctor Blading technique from colloidal pastes as reported previously.[13f,23] The films were annealed at 450 °C for 30 min prior to use, and the anatase phase for TiO_2 was confirmed by X-ray diffraction studies after heating. The resulting film thicknesses, determined by profilometry (Tencor Instruments), were 4 μm. $[Ni(P^{Ph}_2N^{PhCH_2PO(OEt)_2}_2)_2](BF_4)_2$ (**NiP^{Et}**)[7a] (Figure S1, Supporting Information) and **RuP**[24] were prepared according to published procedures.

Physical Measurements. ^1H and ^{31}P NMR spectra were recorded on a Bruker 400 MHz spectrometer. ^1H NMR spectra were referenced to the solvent residual peaks as an internal reference,[25] and ^{31}P NMR spectra were referenced to an external standard (85% H_3PO_4 in D_2O). UV−vis spectra were recorded on a Varian Cary 50 UV−vis spectrophotometer using quartz glass cuvettes. High-resolution electrospray ionization mass spectra (HR-ESI-MS) were recorded on a Quattro LC spectrometer, and the theoretical and experimental isotope distributions were compared. Elemental analysis was carried out by the microanalytical laboratory in the Department of Chemistry of the University of Cambridge.

Synthesis of $[Ni(P^{Ph}_2N^{PhCH_2P(O)(OH)_2}_2)_2]Br_2$·HBr (NiP). Bromotrimethylsilane (0.25 mL, 1.86 mmol) was added dropwise to a deep red solution of **NiP^{Et}** (250 mg, 0.143 mmol) in degassed dichloromethane (15 mL) under a N_2 atmosphere at room temperature. The color changed to deep purple, and the solution was stirred for 2 days at room temperature. The solvent was removed, followed by addition of deoxygenated MeOH (HPLC grade, 15 mL) to the dark solid residue and stirring under N_2 for 1 day at room temperature. The volume of the solvent was reduced to approximately one-third, and the product was precipitated with Et_2O (~25 mL). After the mixture was stirred for 30 min, the deep purple precipitate was filtered off under N_2, washed with Et_2O, and dried in vacuo. The solid was redissolved in MeOH, the solution was stirred for several minutes, and the solvent was evaporated under high vacuum to give a purple solid. Yield: 183 mg (81%). ^1H NMR (400 MHz, CD_3OD, δ): very broad signals, 8.23−6.70 (m, 36H, Ph), 3.60−4.70 (m, 16H, NCH_2P), 2.97−3.22 (m, 8H, $PhCH_2PO(OH)_2$) ppm. $^{31}P\{^1H\}$ NMR (162 MHz, CD_3OD, δ): 25.8 ($PO(OH)_2$), 21.0 (NCH_2P), −13.9 (NCH_2P) ppm. HR-ESI-MS (MeOH, negative): m/z calcd for $[M - 2H + Br]^-$ 1419.1121, found 1419.1154; m/z calcd for $[M - 3H]^-$, 1339.1895, found 1339.1903. Anal. Calcd for $C_{60}H_{68}Br_2N_4NiO_{12}P_8$·HBr·2$H_2O$: C, 44.47; H, 4.54; N, 3.46; P, 15.29; Br, 14.79. Found: C, 44.45; H, 4.70; N, 3.24; P, 14.61; Br, 15.08. UV−vis (MeOH): λ_{max}, nm (ε) 510 (1100).

Electrochemistry. Electrochemical measurements were performed on an IviumStat or Ivium CompactStat potentiostat under an argon atmosphere using a three-electrode configuration. A glassy-carbon disk (3 mm diameter) working electrode, a platinum-wire counter electrode, and a Ag/AgCl/KCl(sat) reference electrode were used for cyclic voltammetry (CV). All potentials were converted to the normal hydrogen electrode (NHE) by addition of +0.197 V.[26]

Controlled-potential electrolysis (CPE) was carried out in a three-necked flask with a three-electrode setup using glassy-carbon rods as working and counter electrodes (surface area in solution ~2 cm^2) and a Ag/AgCl/KCl(sat) reference electrode. A solution of **NiP** (0.18 mM) in ascorbic acid (AA, 0.1 M, pH 4.5) was purged with N_2 containing CH_4 (2%) as the internal gas chromatography (GC) standard, and a potential of −0.5 V vs NHE was applied during CPE for 2 h. The Faradaic yield was calculated from the amount of H_2 accumulated in the headspace, as measured by GC. CPE of catalyst-free electrolyte at the same potential showed no production of H_2.

Preparation of RuP-Sensitized TiO_2 and ZrO_2 Films Loaded with and without NiP for Spectroscopic Studies. To prepare TiO_2 and ZrO_2 films sensitized with **RuP**, an aqueous solution of **RuP** (10 μL of 4 μM) was spread onto the films (geometrical surface area 1.5 cm^2), and the solvent was dried in air for 30 min. For TiO_2 and ZrO_2 films cofunctionalized with **RuP** and **NiP**, first a solution of **NiP** (10 μL of 8 μM) in MeOH was spread onto the surface of the film, followed by drying for 30 min in air. Then, an aqueous **RuP** solution

dx.doi.org/10.1021/ja410592d | J. Am. Chem. Soc. 2014, 136, 356−366

(10 μL of a 4 μM) was spread onto the surface of the film and was dried for an additional 30 min.

Spectroscopic Characterization. Spectroscopic measurements on homogeneous solutions and functionalized TiO_2 and ZrO_2 films were carried out in water or in aqueous AA solution (0.1 M) carefully adjusted to pH 4.5 with NaOH (0.1 M), unless otherwise stated. A fresh AA solution was prepared prior to any measurements. The aqueous solutions were purged with N_2 for 15 min prior to the measurements. The UV−vis and fluorescence spectra of the solutions and films were recorded using a quartz cuvette (1 cm path length) on a Perkin−Elmer Lambda 35 UV−vis spectrophotometer and a Horiba Jobin Yvon Fluorolog luminescence spectrophotometer, respectively. TC-SPC measurements were performed by using a Horiba Jobin Yvon TBX Fluorocube system. As the excitation source, a pulsed laser with 467 nm nominal wavelength at a repetition rate of 100 kHz was used. The photoluminescence intensity of **RuP** at λ_{em} 650 nm was measured as a function of time after the excitation pulse, for a fixed data collection period to ensure matched densities of absorbed photons between samples (600 s). The instrument response was measured at the full width at half-maximum and showed typically a 200−250 ps value. All TC-SPC experiments undertaken on TiO_2 and ZrO_2 films were measured under aqueous conditions or a 0.1 M AA solution at pH 4.5 in air.

The microsecond to second transient absorption decays were measured using a Nd:YAG laser (Big Sky Laser Technologies Ultra CFR Nd:YAG laser system, 6 ns pulse width). The second and third harmonics of the laser (corresponding to 532 and 355 nm, respectively) were used to excite **RuP**. The laser intensity was adjusted using neutral density filters as appropriate, with experiments typically employing 350 μJ cm^{-2}, and the frequency of the laser pulse was fixed to 1 Hz. A liquid light guide with a diameter of 0.5 cm was used to transmit the laser pulse to the sample. The probe light source was a 100 W Bentham IL1 tungsten lamp, and the probing wavelength was selected by using a monochromator (OBB-2001, Photon Technology International) placed prior to the sample. Several high-pass, low-pass and neutral-density filters (Comar Optics) were used to decrease the light arriving to the detector. Transient absorption data were collected with a Si photodiode (Hamamatsu S3071). The information was passed through an amplifier box (Costronics) and recorded using a Tektronics TDS 2012c oscilloscope (microsecond to millisecond time scale) and a National Instruments (NI USB-6211) DAQ card (millisecond to second time scale). The decays observed were the average of 500 laser pulses. The data were processed using home-built software based on Labview.

Photocatalytic H_2 Evolution Experiments. All photocatalytic experiments were carried out using a Solar Light Simulator (Newport Oriel, 100 mW cm^{-2}) equipped with an air mass 1.5 global filter (AM 1.5G). UV irradiation was filtered using a 420 nm cutoff filter (UQG optics), and IR irradiation was filtered by a water filter (path length 10 cm). The photoreactor was held at a constant temperature of 25 °C in all experiments. Samples were generally prepared in air protected from light by an Al foil. The reaction vessel was sealed with a rubber septum, and air was replaced by N_2 containing 2% CH_4 (internal GC standard). The irradiated cross section of the solution in the vials was approximately 3.3 cm^2. H_2 evolution was monitored by GC measurements with an Agilent 7890A Series GC equipped with a 5 Å molecular sieve column. The GC oven temperature was kept constant at 45 °C, N_2 was used as a carrier gas at an approximate flow rate of 3 mL min^{-1}, and a thermal conductivity detector (TCD) was used. Samples (15−20 μL) for headspace gas analysis were taken from the reaction vessel headspace in 30 min intervals for 2 h in the screening experiments. For long-term measurements longer intervals were chosen. The response factor of the thermal conductivity detector for H_2 compared to CH_4 was 1.91.

Preparation of Homogeneous System RuP-NiP. In a typical experiment, a freshly prepared AA solution was titrated to the desired pH using NaOH (0.1 M) or HBF_4 (0.1 M) and diluted to a final AA concentration of 0.1 M (the final pH was confirmed). Stock solutions of **RuP** (1.0 or 2.0 mM in H_2O) and **NiP** (2.0 mM in MeOH) were added in the desired ratio to the aqueous AA solution (0.1 M) to reach a final volume of 2.25 mL, leaving 5.59 mL of gas headspace in the vial. Control experiments in the absence of MeOH were carried out and confirmed a comparable photocatalytic activity.

Immobilization of RuP and NiP on TiO_2 and ZrO_2: RuP-TiO_2-NiP and RuP-ZrO_2-NiP. AA (0.1 M) was prepared as described above. ZrO_2 or TiO_2 nanoparticles (2.5 mg) were placed in a vial containing an AA solution and dispersed by sonication for 5 min. To load the particles, first **NiP** was added and after stirring for several min **RuP** was added, resulting in a final volume of 2.25 mL, leaving 5.59 mL of gas headspace in the vial.

Quantification of Catalyst Loading on the Nanoparticles by UV−Vis Spectrophotometry. The adsorption of **NiP** on TiO_2 and ZrO_2 nanoparticles was quantified by recording the difference UV−vis spectrum of a solution of **NiP** in AA (0.1 M, pH 4.5, 2.25 mL) before and after exposure to TiO_2 or ZrO_2 nanoparticles (2.5 mg). The solution was stirred with the nanoparticles for 30 min, followed by centrifugation (7000 rpm, 5 min) between the measurements. Adsorption of **RuP** on nanoparticles after coadsorption with **NiP** was estimated by adding **RuP** (0.05 μmol) to a suspension of **NiP**-sensitized TiO_2 or ZrO_2 particles (0.02 or 0.1 μmol **NiP** loading on 2.5 mg nanoparticles). The suspensions were purged with N_2 during catalyst loading. Quantitative adsorption of 0.05 μmol **RuP** and 0.02 μmol **NiP** would result in an estimated surface coverage of approximately 400 **RuP** and 150 **NiP** molecules per nanoparticle and approximately 45% coverage of the TiO_2 surface (see the Supporting Information).

Determination of Photon to H_2 Quantum Efficiency. The external quantum (photon to H_2 conversion) efficiency (EQE) was determined by an LED light source (Modulight, Ivium) using blue light (λ 460 nm, 5 mW cm^{-2}). The light intensity was measured with a Newport thermopile detector (818P-020-12) coupled with an optical power meter (1916-R). Samples of **RuP** (0.3 μmol) and **NiP** (0.1 μmol) in solution were used. Aliquots of headspace gas were subjected to GC analysis during irradiation. The efficiency was determined from the amount of H_2 produced after 2 h of irradiation using the equation

$$\mathrm{EQE}\ (\%) = \frac{(\mathrm{H_2}(2\ \mathrm{h})/\mathrm{mol}) \times 2}{\mathrm{photons}(2\ \mathrm{h})/\mathrm{einstein}} \times 100$$

Treatment of Data. All analytical measurements were repeated at least three times. The obtained data were treated as follows: for a sample of n observations x_i, the unweighted mean value x_0 and the standard deviation σ were calculated using the equations

$$x_0 = \sum_i \frac{x_i}{n} \qquad \sigma = \sqrt{\sum_i \frac{(x_i - x_0)^2}{(n-1)}}.$$

A minimum σ of 10% was assumed in all experiments. The light sources and gas chromatographs were calibrated regularly to ensure reproducibility throughout all experiments.

RESULTS AND DISCUSSION

Synthesis and Characterization of NiP. The catalyst **NiP** was synthesized through hydrolysis of the octaethyl phosphonate ester analogue $\mathbf{NiP^{Et}}$ [7a] by dealkylation of the ethyl ester groups with trimethylsilyl bromide in dichloromethane[27] (Figure S1, Supporting Information). **NiP** was obtained in 81% yield and characterized by ^1H and ^{31}P NMR spectroscopy, high-resolution mass spectrometry, and elemental analysis for C, H, N, P, and Br. **NiP** is soluble in water (~0.3 mg mL^{-1}) and dissolves well in an aqueous ascorbic acid solution (0.1 M, pH 4.5) with a solubility of more than 5 mg mL^{-1}. **NiP** therefore is an example of a DuBois-type Ni catalyst that is soluble in aqueous solutions and can be employed homogeneously in organic solvent free aqueous catalytic systems.

Electrocatalytic Activity of NiP in Aqueous Solution. Before studying **NiP** in a purely aqueous electrolyte solution, we compared **NiP** with the previously studied complex $\mathbf{NiP^{Et}}$

dx.doi.org/10.1021/ja410592d | J. Am. Chem. Soc. 2014, 136, 356−366

(Figure S1)[7a] in acetonitrile/water mixtures and in the presence of added triflic acid. On a glassy-carbon working electrode under Ar at a scan rate of 100 mV s^{-1}, CV measurements of **NiP** (0.3−0.5 mM) show two quasi-reversible waves at $E_{1/2}$ = −0.38 and −0.54 V vs NHE in H_2O (0.1 M Na citrate pH 5)/acetonitrile (0.1 M $TBABF_4$) (1/1). The two waves are assigned to the $Ni^{II/I}$ and $Ni^{I/0}$ redox couples, respectively (Figure 2A and Figures S2 and S3 (Supporting Information)).[4g]

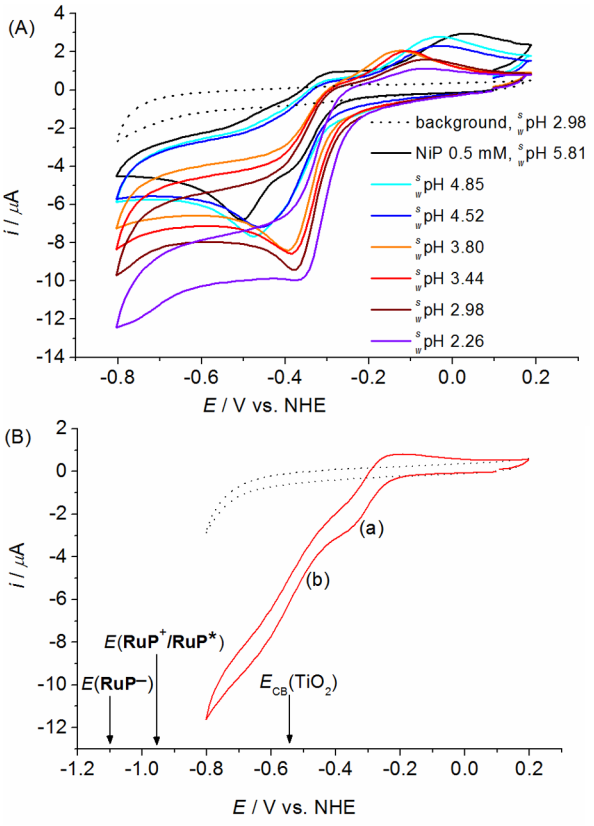

Figure 2. (A) CV of **NiP** (0.5 mM, black trace) in H_2O (0.1 M Na citrate pH 5)/acetonitrile (0.1 M $TBABF_4$) (1/1), followed by titration with increasing amounts of triflic acid (0.678 M in H_2O). $^{s}_{w}$pH is the concentration of protons in a mixed solvent (water/organic solvent) where the pH was measured in water against an aqueous reference.[28] (B) CV of **NiP** (0.3 mM, solid red trace) in an aqueous AA solution (0.1 M, pH 4.5). Wave (a) shows the first reduction wave of **NiP**, and wave (b) indicates the onset of catalytic proton reduction. Reduction potentials of possible reactive intermediates of **RuP** in a photocatalytic process and the conduction band potential of TiO_2 ($E_{CB}(TiO_2)$) are also shown. A glassy-carbon working electrode, a Ag/AgCl/KCl(sat.) reference electrode, and a platinum-wire counter electrode were employed at room temperature with a scan rate of 100 mV s^{-1} in (A) and (B). Control experiments in the absence of **NiP** are shown as dashed traces.

Addition of triflic acid induced a catalytic current attributed to proton reduction below $^{s}_{w}$pH[28] ~4.9 following the reduction of Ni^{II} to Ni^{I} with an onset potential of −0.3 V vs NHE (Figure 2A). The small cathodic shift in potential of the reduction wave upon acidification is presumably due to protonation of the dangling phosphonate moieties. Thus, the $[Ni(P_2^{R\prime}N_2^{R\prime\prime})_2]^{2+}$ core and electrocatalytic proton reduction activity are intact in **NiP** and the electrochemical response is indeed comparable to that of $\mathbf{NiP}^{Et}$ in the presence of an organic acid (Figures S2−S4, Supporting Information).

Electrocatalytic proton reduction by **NiP** was also observed in the absence of organic solvent in an aqueous solution buffered with ascorbic acid (AA) or Na citrate (0.1 M, pH 4.5). A single, irreversible reduction wave (a) was observed at E_p = −0.35 V vs. NHE, followed by the onset of a catalytic wave (b) at approximately −0.48 V vs NHE (Figure 2B and Figure S5 (Supporting Information)). Therefore, the catalyst operates with a small overpotential requirement of approximately 0.2 V in comparison to the thermodynamic potential for proton reduction of −0.27 V vs NHE at pH 4.5. The reduction potentials of intermediates of **RuP**, which are likely to be formed during the quenching process after photoexcitation (see below) are also indicated in Figure 2B. The position of these potentials and the conduction band edge of TiO_2 suggest that enough driving force for photocatalytic proton reduction with **NiP** would be available when using **RuP** and **RuP**-sensitized TiO_2 as a light harvester, as described in detail in the kinetic and photocatalytic sections.

Controlled-potential electrolysis with **NiP** (0.18 mM) in an aqueous ascorbic acid solution (0.1 M, pH 4.5) on a glassy-carbon-rod working electrode (surface area ~2 cm^2) at −0.5 V vs NHE for 2 h confirmed the generation of H_2 gas with a Faradaic yield of 85 ± 4% (H_2 in the headspace quantified by GC). Rinsing the electrode with H_2O after CPE and immersing it in a fresh electrolyte solution (in the absence of **NiP** catalyst) did not result in the formation of H_2 when continuing with CPE at the same potential. Thus, H_2 production originates from a dissolved catalyst and not from electrodeposited decomposition products on the electrode. Thus, the water-soluble **NiP** displays electroactivity for the reduction of aqueous protons with a high Faradaic yield in the absence of organic solvents, a prerequisite for the use of **NiP** in photocatalytic schemes in water.

Kinetics and Mechanisms of ET in Photocatalytic Schemes. The suitability of **NiP** in photocatalytic H_2 generation was studied with **RuP**,[24,29] AA (0.1 M) as a sacrificial electron donor, and buffer (pK_a 4.17) in aqueous solution.[30] Photoexcitation of **RuP** to **RuP*** (λ_{max} 455 nm, MLCT) can result in either oxidative or reductive quenching of the photoexcited state (Figures 3 and 4).[31] First, the kinetics and mechanisms of ET between **RuP** and **NiP** in homogeneous aqueous solution (**RuP**-**NiP** system) and anchored onto metal

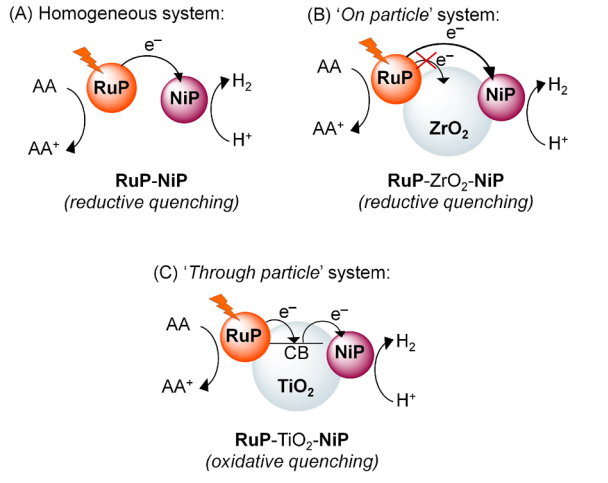

Figure 3. Three distinct photosystems with homogeneous and heterogenized catalysts studied herein. See Figure 4 for kinetic and mechanistic details.

dx.doi.org/10.1021/ja410592d | J. Am. Chem. Soc. 2014, 136, 356−366

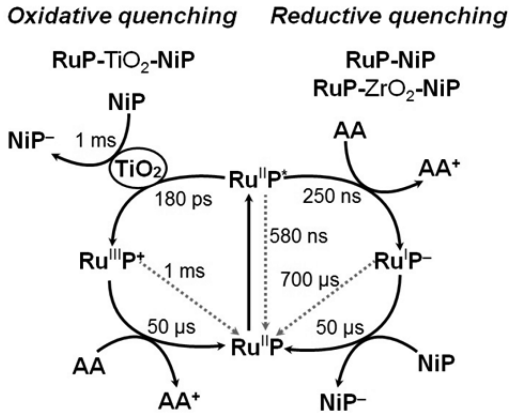

Figure 4. Summary of ET kinetics for the three photocatalytic systems studied as determined by TC-SPC and TAS (defined as $t_{50\%}$ times). Recombination reactions are represented with dashed gray arrows.

oxide surfaces (**RuP**-ZrO_2-**NiP** and **RuP**-TiO_2-**NiP** systems) were studied by TC-SPC and TAS. The three photocatalytic systems are illustrated in Figure 3, and the mechanistic and kinetic details are summarized in Figure 4 and described below. The **RuP**-**NiP** and **RuP**-ZrO_2-**NiP** systems generate H_2 through a reductive quenching mechanism of **RuP** in solution or "on the particle", respectively. **RuP**-TiO_2-**NiP** undergoes oxidative quenching and electrons are transferred "through the particle".

TiO_2 was observed to cause oxidative quenching of the immobilized **RuP***, resulting in the oxidized intermediate **RuP**$^+$ (E(**RuP**$^+$/**RuP***) = −0.95 V vs NHE)[32] by electron injection into the conduction band of TiO_2 (E_{CB} = −0.55 V vs NHE at pH 4.5).[33] These kinetics were measured by TC-SPC to take place in approximately 180 ps, with an injection efficiency of >95% (Figure 5).[13f]

The transient absorption spectrum of a photoexcited **RuP**-TiO_2 film shows a maximum transient absorption peak at 700 nm, corresponding to the absorption spectrum of the oxidized **RuP**$^+$ (Figure S6, Supporting Information). In the absence of AA, the TiO_2 conduction band electrons recombine with **RuP**$^+$ within approximately 1 ms. Upon reduction of **RuP**$^+$ by AA ($t_{50\%} \approx 50$ μs), corresponding to the regeneration of **RuP**, the resulting photoinjected TiO_2 electrons exhibit a lifetime of 0.5 s. Following the codeposition of **NiP** (molecular ratio **RuP**/**NiP** of 1/2), the decay of these electrons is accelerated to approximately 1 ms, assigned to ET to **NiP** (Figure S7, Supporting Information).

The oxidative ET mechanism from **RuP** to **NiP** through the semiconductor ("through particle" system, Figure 3C), is possible with TiO_2 but not with ZrO_2, due to the energetic mismatch between **RuP*** and the conduction band of ZrO_2 (E_{CB} = −1.26 V vs NHE at pH 4.5).[34] ZrO_2 is therefore unable to accept electrons from **RuP*** and can only be used as a matrix to immobilize the compounds in close proximity on the particle ("on particle" system, Figure 3B).

The reductive quenching through intermolecular ET from AA (E = 1.17 V vs NHE)[35] to **RuP*** (E(**RuP***/**RuP**$^-$) = 1.08 V vs NHE)[31] was measured by TC-SPC to take place in approximately 250 ns with an estimated efficiency of 70% in homogeneous **RuP**-**NiP** and heterogenized "on particle" **RuP**-ZrO_2-**NiP** systems (Figure 5).[36] Photoexcitation of an aqueous **RuP** solution (4 μM) containing AA (0.1 M, pH 4.5) resulted in the appearance of a transient absorption peak at 500 nm

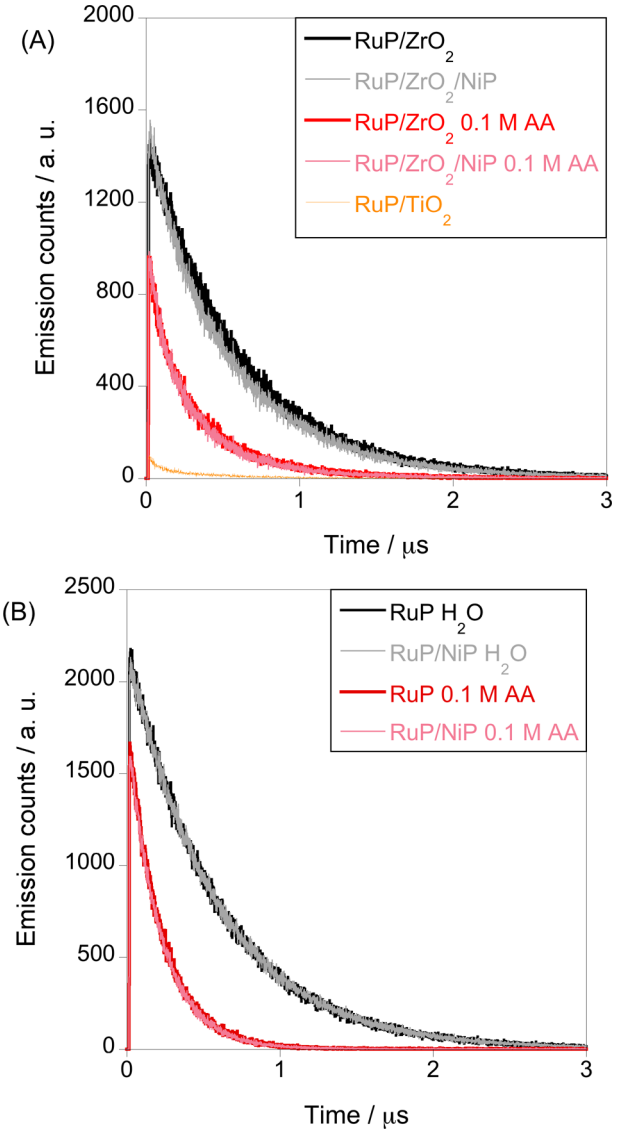

Figure 5. Time-resolved luminescence measurements of **RuP** with and without **NiP** in water and in the presence of AA (0.1 M) at pH 4.5: (A) anchored onto the surface of a TiO_2 and ZrO_2 film (10 μL of 4 μM **RuP**, 10 μL of 8 μM **NiP**); (B) in a homogeneous solution ([**RuP**] = 4 μM, [**NiP**] = 8 μM).

(Figure S8, Supporting Information) assigned to the formation of the reactive intermediate **RuP**$^-$.[37] This reduced state of the dye, **RuP**$^-$, is a strong reducing agent and has a large driving force for the reduction of **NiP** (E(**RuP**/**RuP**$^-$) = −1.09 V vs NHE, Figure 2).[31]

The addition of increasing amounts of **NiP** (from 0 to 16 μM) to a solution containing **RuP** (4 μM) and AA (0.1 M, pH 4.5) results in the linear decrease of the lifetime of **RuP**$^-$ from 700 to 29 μs, following first-order kinetics with respect to **NiP** concentration for the intermolecular ET between **RuP**$^-$ and **NiP** (Figure 6). The second-order rate constant of this ET is $k_{ET} = 1.4 \times 10^9$ M^{-1} s^{-1}, indicating that the ET kinetics are diffusion limited (Figure 6B and Table S1 (Supporting Information)). In addition, the presence of **NiP** resulted in the appearance of a long-lived ($t_{50\%} \approx 0.1$ s) bleaching signal assigned to the reduction of Ni^{II} species (Figure S9 (Supporting Information)) upon reduction by **RuP**$^-$. Further experiments

dx.doi.org/10.1021/ja410592d | J. Am. Chem. Soc. 2014, 136, 356−366

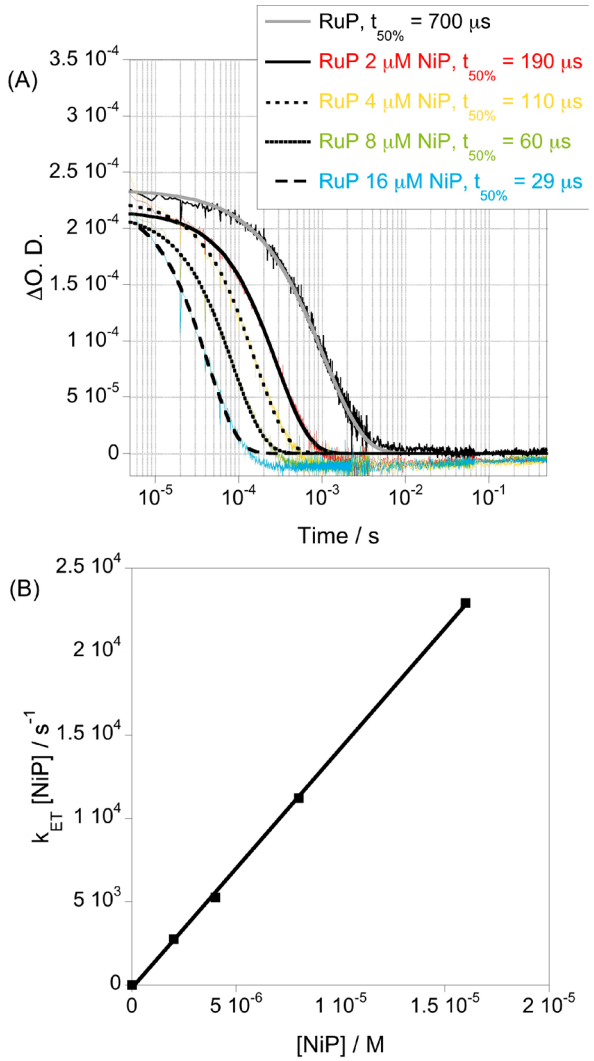

Figure 6. (A) Transient absorption decays of **RuP** (4 μM) in an aqueous AA solution (0.1 M, pH 4.5) after addition of different concentrations of **NiP** (0, 2, 4, 8, and 16 μM). The excitation wavelength was λ_{ex} 532 nm, and the decays were probed at λ_{probe} 500 nm. The data were fitted to stretched exponential equations. (B) Calculated pseudo-first-order rate constant (k_{ET}[**NiP**]) for the ET from **RuP**$^-$ to **NiP** as a function of the concentration of **NiP** catalyst (Table S1 (Supporting Information)). See the caption to Table S1 for details of the analysis.

are ongoing to monitor the nickel catalytic species involved in the H^+ reduction reaction.

The reductive quenching of **RuP*** also occurs through intermolecular ET from AA to **RuP*** in **RuP**-ZrO_2-**NiP**. The photoluminescence intensity and lifetime of **RuP*** on nanostructured ZrO_2 films decrease upon the addition of an aqueous AA solution (0.1 M, pH 4.5), and TC-SPC measurements reveal that reductive quenching of **RuP*** to form **RuP**$^-$ occurs in approximately 250 ns with an estimated ET efficiency of 70% (Figure 5B). The cofunctionalization of ZrO_2 with **NiP** (8 μM) and **RuP** (4 μM) in water does not affect the luminescence of **RuP**, indicating that ET between the two molecules requires the formation of **RuP**$^-$ in the presence of a sacrificial electron donor. A transient absorption peak at 500 nm corresponding to the signal of **RuP**$^-$ was also observed in the **RuP**-ZrO_2 system in the presence of AA (0.1 M at pH 4.5), with the decay of **RuP**$^-$ accelerating following the codeposition of **NiP** (Figure S10 (Supporting Information)). It can be concluded that the same reductive ET mechanism and similar kinetics (dependent upon component loadings/concentrations) take place both in homogeneous media and on anchoring of the molecules onto the surface of a material that does not allow for dye electron injection. Although the reductive ET mechanism is the same for both homogeneous and the "on-particle" ZrO_2 systems, charge separation is achieved through two different processes: while in homogeneous media charge separation occurs through the diffusion of molecules into the solution, when the dye and catalyst are immobilized in **RuP**-ZrO_2-**NiP** charge separation can take place through the intermolecular ET between neighboring molecules.[38]

Standard Conditions for Photocatalytic H_2 Evolution. The spectroscopic studies revealed that all three photocatalytic systems drive the efficient photoreduction of **NiP**. We subsequently studied photocatalytic generation with **NiP** in bulk experiments. All three systems were indeed efficient in producing H_2 during irradiation with visible light. Consequently, the systems were studied and optimized by varying the pH value of the AA solution and concentrations of **RuP** and **NiP** (Table 1 and Tables S2–S4 (Supporting Information)). The photocatalytic activity and longevity of H_2 production was dependent on the conditions and type of system employed. The photocatalytic performance of **NiP** generally varied in all three environments, and the rate of photogenerated H_2 was constant over at least 1 h in all experiments (Figure 7A). The turnover frequencies based on **NiP** (TOF_{NiP}) were calculated from the amount of H_2 accumulated in a photoreactor after 1 h irradiation (Tables S3 and S4).

Photo-H_2 Generation with Homogeneous RuP-NiP. In a homogeneous **RuP**-**NiP** system, a TOF_{NiP} value of 460 ± 60 h^{-1} was observed when **RuP** (0.05 μmol) was used with a low amount of **NiP** (0.02 μmol) in aqueous AA (0.1 M, 2.25 mL). This **RuP**-**NiP** system was photoactive for 2 h with a final TON_{NiP} value of 723 ± 171 (15 ± 3 μmol of H_2). An increasing amount of **NiP** (0.1 μmol) resulted in a decreased initial TOF_{NiP} concomitant with an increased system lifetime and a comparable overall TON_{NiP} value of 651 ± 30 (65 ± 3 μmol of H_2) after 30 h irradiation (Table 1 and Figure 7B). This observation might be explained by the less likely double reduction of a single molecular catalyst at high **NiP** concentrations. Addition of **RuP** or AA to a photodegraded system did not result in reactivation, suggesting that decomposition of **NiP** occurred after approximately 700 TONs. Addition of **NiP** to a deactivated homogeneous system did result in reactivation, but full photoactivity was not restored, indicating that photodegradation affected not only **NiP** but also other system components such as **RuP**. Indeed, photobleaching of **RuP** became evident after 1 h irradiation by recording an electronic absorption spectrum of the homogeneous solution after irradiation in a gastight quartz cuvette under standard conditions (Figure S11 (Supporting Information)).

Several sets of control experiments were carried out, which showed that no or only negligible amounts of H_2 were produced in the absence of **RuP**, **NiP**, AA or light. The presence of additional buffers such as citrate and acetate did not impede the photocatalytic activity of the original system. Replacement of **NiP** by different Ni salts such as $NiCl_2$ and $NiBr_2$ in combination with 4 equiv of a water-soluble phosphine ([2-(dicyclohexylphosphino)ethyl]trimethylammonium chloride) resulted only in negligible amounts of H_2. Homogeneous

dx.doi.org/10.1021/ja410592d | J. Am. Chem. Soc. 2014, 136, 356–366

Table 1. Visible-Light-Driven H_2 Production with RuP and NiP in Homogenous Solution and Coimmobilized on TiO_2 and ZrO_2

conditions[a]	$TOF_{NiP} \pm \sigma/h^{-1}$	$H_2 \pm \sigma/\mu$mol (after 2 h)	TON_{NiP}	lifetime/h
RuP Dependence[b]				
0.025 μmol of **RuP**	64 ± 10	14.3 ± 1.3	>142	>2
0.3 μmol of **RuP**	236 ± 21	50.0 ± 2.3	>500	>2
0.5 μmol of **RuP**	297 ± 48	62.1 ± 6.3	>620	>2
Replacement of **RuP** by Organic Dye				
Eosin Y (0.3 μmol), **NiP** (0.1 μmol), AA (0.1 M, pH 4.5)	189 ± 31[f]	12.3 ± 3.5		
pH Dependence[c]				
pH 4.0	185 ± 25	41.2 ± 3.4	>412	>2
pH 4.5	236 ± 21	50.0 ± 2.3	>500	>2
pH 5.0	210 ± 24	33.4 ± 0.4	>334	>2
NiP Dependence[d]				
RuP-NiP (0.02 μmol of **NiP**)	460 ± 60	14.5 ± 3.4	723 ± 171	2
RuP-NiP (0.1 μmol of **NiP**)	104 ± 10	22.0 ± 1.2	651 ± 30	30
RuP-ZrO_2-**NiP** (0.02 μmol of **NiP**)	27 ± 3	0.9 ± 0.03	>43	>2
RuP-ZrO_2-**NiP** (0.1 μmol of **NiP**)	92 ± 26	16.1 ± 1.4	524 ± 36	30
RuP-TiO_2-**NiP** (0.02 μmol of **NiP**)	51 ± 7	1.7 ± 0.2	>85	>2
RuP-TiO_2-**NiP** (0.1 μmol of **NiP**)	72 ± 5	13.8 ± 0.3	278 ± 19	30
Control Experiments − Homogeneous System				
no **RuP**, **NiP** (0.1 μmol) in AA (0.1 M, pH 4.5)		g		
RuP (0.3 μmol), **NiP** (0.1 μmol), Na citrate (0.1 M, pH 4.5), no AA		g		
Control Experiments − Heterogenized Systems[e]				
no **NiP**, **TiO_2**, **RuP** (0.05 μmol), AA (0.1 M, pH 4.5)		g		
no **NiP**, **ZrO_2**, **RuP** (0.05 μmol), AA (0.1 M, pH 4.5)		g		

[a]All samples were irradiated with visible light (AM 1.5 G filter, 100 mW cm^{-2}, λ >420 nm, 25 °C) under an N_2 (2% CH_4) atmosphere and a standard solvent volume of 2.25 mL, leaving a gas headspace volume of 5.59 mL. Standard screening samples were irradiated for 2 h in AA (0.1 M, pH 4.5), and the TOF was determined after 1 h irradiation. [b]Homogeneous system with **NiP** (0.1 μmol) and different amounts of **RuP**. [c]Homogeneous system with **NiP** (0.1 μmol), **RuP** (0.3 μmol), and different pH values. [d]**RuP** (0.05 μmol); in heterogenized systems TiO_2 or ZrO_2 (2.5 mg per sample) nanoparticles were used as dispersions. [e]TiO_2 or ZrO_2 nanoparticles (2.5 mg per sample). [f]TOF_{NiP} after 15 min visible light irradiation reported due to rapid bleaching of Eosin Y. [g]No H_2 detected in GC measurements (limit of detection <0.01%).

systems using commercially available dyes such as $[Ru(bipy)_3]Cl_2$ (TOF_{NiP} = 220 ± 20 h^{-1}) or the organic, noble-metal-free dye Eosin Y (used as the disodium salt; TOF_{NiP} = 189 ± 31 h^{-1}) also resulted in efficient photocatalytic H_2 production in an aqueous AA solution (0.1 M, pH 4.5) (Table 1 and Table S6 (Supporting Information)).

Photon-to-H_2 Conversion Efficiency. The external quantum efficiency (EQE) of the homogeneous photocatalytic system with **RuP** (0.3 μmol) and **NiP** (0.1 μmol) in AA (0.1 M, pH 4.5) was measured using an LED light source (λ 460 nm, 5 mW cm^{-2}). An EQE value of 9.7 ± 1.2% was determined after 2 h irradiation. We note that this external yield assumes that all photons emitted by the light source were absorbed by **RuP** and therefore represents a lower estimate of the quantum efficiency of the system. The photon-to-H_2 quantum yield observed for our homogeneous **RuP-NiP** system is remarkable in comparison to other photocatalytic systems with molecular 3d transition-metal catalysts operating homogeneously or immobilized in aqueous solution. Recently reported quantum yields for homogeneous photocatalytic systems ranged from 0.23 to 0.6% for a Co-pentapyridine catalyst with $[Ru(bpy)_3]^{2+}$ as photosensitizer[39] in an aqueous system at neutral pH to 4.6% for a cobaloxime-based H_2 generation system with an Al-porphyrin dye in a water/acetone solvent system.[13k] In systems with a molecular catalyst immobilized on a solid-state material, EQEs of approximately 1−1.5% for a cobaloxime immobilized on **RuP**-sensitized TiO_2[13f] and a $Ni(TEOA)_3^{2+}$ (TEOA = triethanolamine) complex on graphitic carbon nitride,[40] respectively, were reported.

EQEs for self-assembled photocatalytic systems using Ni salts and 2-mercaptoethanol (24.5%)[4f] or dihydrolipoic acid (36% QE)[14] ligands are still benchmarks; however, a defined catalytically active species has not been reported for these systems.

Benchmark for Synthetic Photochemical Systems. Various homogeneous photocatalytic schemes have been reported for the reduction of aqueous protons with molecular catalysts. Examples of efficient photo-H_2 generating systems include a molecular dye combined with $[Ni(P_2^{R'}N_2^{R''})_2]^{2+}$-type[4g] and Fe-based molecular catalysts,[3c,15] but in these systems water/organic solvent mixtures were employed. Photocatalytic schemes for H_2 generation which operate in pure aqueous systems are highly desirable.[11] Very recently, the water-insoluble $[Ni(P_2^{Ph}N_2^{Ph})_2](BF_4)_2$ was incorporated into the photosynthetic protein Photosystem I (PSI) for photocatalytic H_2 production in aqueous solution,[19b] but only a very limited amount of Ni catalyst can be loaded onto dilute enzyme systems and the photostability of the hybrid assembly remained an issue (more than half of the photoactivity ceased after 30 min of irradiation).

Nickel-thiolate[4i] and cobalt-dithiolene[13l] catalysts have been reported to achieve several thousand turnovers in organic solvent/water mixtures. Cobaloximes have been reported to evolve H_2 in a homogeneous system[13g] and on **RuP**-sensitized TiO_2 in water,[13f] but the TOF_{Co} value never exceeded 20 h^{-1} and the photon-to-H_2 efficiency was only 1%. The higher photocatalytic activity and EQE of **NiP** in comparison to those of cobaloxime catalysts may be related to the similar reduction

dx.doi.org/10.1021/ja410592d | J. Am. Chem. Soc. 2014, 136, 356−366

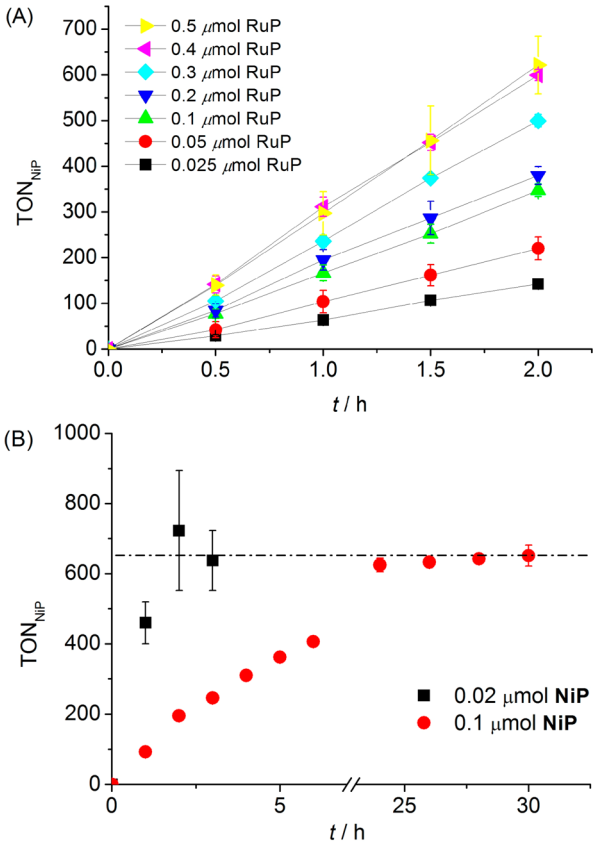

Figure 7. (A) Visible-light-driven generation of H_2 in a homogeneous aqueous system (0.1 M AA, pH 4.5) comprised of (A) **NiP** (0.1 μmol) with different amounts of **RuP** and (B) **RuP** (0.05 μmol) with low (0.02 μmol, squares) and high loadings of **NiP** (0.1 μmol, circles).

potentials required for both reduction steps in **NiP**. We have previously shown that the photocatalytic activity of a cobaloxime complex is significantly limited by its relatively slow second reduction kinetics, attributed at least in part to the relatively unfavorable energetics for this second reduction.[41] The use of a Co-pentapyridine catalyst[39] and a [FeFe]-hydrogenase mimic[12a] in photocatalytic schemes in an aqueous solution resulted in TOFs of approximately 20 and 50 h^{-1}, respectively. Thus, our **RuP**-**NiP** system compares favorably with previously reported systems in organic solvent free aqueous solution.

Photo-H_2 Generation with Heterogenized Catalysts. The immobilization of a molecular catalyst on a photoelectrode is a prerequisite for fuel generation in a photoelectrochemical device, and the attachment on a semiconductor material is particularly desirable. Therefore, we extended our studies using **NiP** for H_2 generation in heterogeneous photocatalytic assemblies with nanoparticle suspensions as a first step towards an electrode assembly.

We first determined the maximum loading capacity of **RuP**[6c] and **NiP** on the metal oxide particles by spectrophotometry. Approximately 0.05 μmol of **RuP** or **NiP** can be immobilized per milligram of TiO_2 or ZrO_2 when adding an excess of phosphonated catalyst (see the Supporting Information).[6c,13f]

The metal oxide nanoparticles were loaded by the following procedure: **NiP** was added to a suspension of TiO_2 or ZrO_2 in aqueous AA solution (2.5 mg in 2.25 mL), and then **RuP** was added. **NiP** was loaded first due to the optimized geometry of adsorption of phosphonated bipyridine ligands of **RuP**.[29b] The photoactivity of the suspensions was studied under irradiation with visible light (AM1.5G, 100 mW cm^{-2}, λ >420 nm). Upon investigating the heterogeneous photocatalytic systems, notably different trends in performance were observed in comparison to the homogeneous system at lower **NiP** loadings (Figure 8).

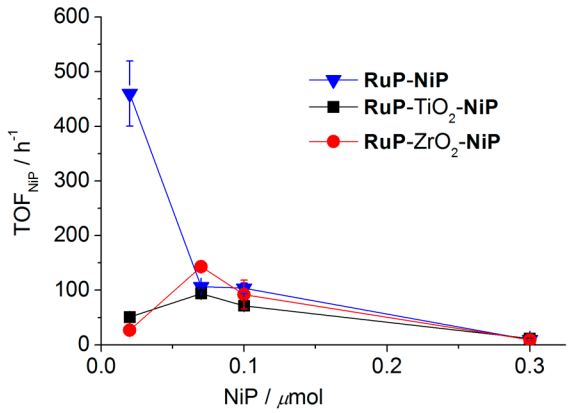

Figure 8. Visible-light-driven H_2 evolution rate with different amounts of **NiP** and **RuP** (0.05 μmol): (triangle) **RuP**-**NiP**; (square) **RuP**-TiO_2-**NiP**; (circle) **RuP**-ZrO_2-**NiP**.

In a **RuP**-ZrO_2-**NiP** system, a low amount of **NiP** (0.02 μmol) with **RuP** (0.05 μmol) on 2.5 mg of ZrO_2 resulted in a TOF_{NiP} value of 27 ± 3 h^{-1}. The results obtained in TAS measurements suggest that direct interaction of the quenched dye (**RuP**$^-$) with **NiP** is required to drive the reaction. ET between **RuP** and **NiP** "on the particle" as observed by the spectroscopic studies above becomes difficult under such dilute conditions due to the spatial separation of the compounds on the ZrO_2 surface. When the amount of **NiP** added to ZrO_2 is increased to 0.1 μmol, a significant enhancement in TOF_{NiP} to 92 ± 26 h^{-1} was observed (Figure 8 and Table S4 (Supporting Information)).

We note that, at low concentrations of compounds carrying phosphonic acid groups, attachment on ZrO_2 or TiO_2 is not quantitative, presumably due to competitive binding of AA to metal oxides.[42] Spectrophotometric studies indicate that **NiP** is almost quantitatively (>80%) adsorbed on ZrO_2, whereas only approximately 10% of **RuP** adsorbs on **NiP**-modified ZrO_2 (Table S7 (Supporting Information)). When the ZrO_2 nanoparticles were loaded with **NiP** (0.02 μmol) and **RuP** (0.05 μmol), separated by centrifugation, and redispersed in fresh AA (0.1 M, pH 4.5), the amount of H_2 produced was 0.16 μmol after 1 h irradiation (in comparison to 0.54 μmol of H_2 before centrifugation). Thus, the photodriven H_2 production in bulk experiments can best be described as a mixture of ET between surface-immobilized catalysts through an "on particle" mechanism[38] and from solubilized **RuP**$^-$ to surface-bound **NiP**.

A **RuP**-TiO_2-**NiP** system displays a TOF_{NiP} value of 51 ± 7 h^{-1} at a low **NiP** loading of 0.02 μmol on 2.5 mg of TiO_2 (Table 1). The rate of H_2 production reached a maximum with a **NiP** loading of 0.1 μmol, whereupon a TOF_{NiP} value of 72 ± 5 h^{-1} and an overall TON_{NiP} value of 278 ± 19 h^{-1} (after 30 h) was obtained (Table S5 (Supporting Information)).

Under these conditions, at least 80% of **NiP** and more than 20% of **RuP** are attached on TiO_2, as measured by spectrophotometry (Figures S12 and S13 (Supporting Information)). Once **NiP** or **RuP** is bound to the TiO_2 surface, it cannot easily be removed from the solid-state

dx.doi.org/10.1021/ja410592d | J. Am. Chem. Soc. 2014, 136, 356−366

material. Redispersion of loaded particles in a fresh AA solution did not result in the detection of significant amounts of **RuP** or **NiP** in solution. Loading the TiO_2 nanoparticles with **NiP** (0.02 μmol) and **RuP** (0.05 μmol), centrifugation, and resuspension in fresh AA (0.1 M, pH 4.5) resulted in a TOF_{NiP} value of 24 h^{-1} during irradiation. Thus, 50% of the photocatalytic activity remained, thereby establishing the importance of the role of the conduction band and the "through particle" mechanism observed in the spectroscopic study. This experiment and the significantly higher rate of photocatalytic H_2 production for **RuP**-TiO_2-**NiP** in comparison to **RuP**-ZrO_2-**NiP** at very low loading of the particles with **NiP** (Table 1) support a preferential "through particle" ET mechanism for TiO_2: a mechanism which does not require the direct electronic communication of **RuP** and **NiP** as needed on ZrO_2.

These results show that photocatalytic H_2 production can be achieved with a DuBois-type catalyst attached on a solid-state semiconductor. However, to this point limitations by the loading capacity of materials used and by competitive binding of electron donor or electrolyte are still being faced when investigating such hybrid materials. Work is in progress to overcome these limitations by investigating the binding modes of the molecular components and photocatalytic activity of **RuP**-**NiP** systems on thin films and electrode materials.

CONCLUSIONS

In summary, we describe a novel $[Ni(P^{R'}_2N^{R''}_2)_2]^{2+}$-type H_2 evolution catalyst (**NiP**), which is soluble in water and can be immobilized on metal oxide surfaces. **NiP** is electrocatalytically active in organic solvent free aqueous solution and evolves H_2 with an onset potential of only −0.48 V vs NHE under mild conditions (pH 4.5). Photocatalytic and spectroscopic studies were performed with **NiP** in three different systems in a purely aqueous solution containing AA. A homogeneous **RuP**-**NiP** system operates through reductive quenching of **RuP*** in solution. The heterogeneous **RuP**-ZrO_2-**NiP** system shows the same ET mechanism, and ZrO_2 acts merely as a matrix to retain the attached molecules closely together, hence facilitating ET "on the particle". In **RuP**-TiO_2-**NiP**, ET occurs via a "through particle" mechanism, where **RuP*** is oxidatively quenched upon injection of an electron into the conduction band of TiO_2, which can subsequently be harvested by **NiP**.

A high TOF value of 460 ± 60 h^{-1} for light-driven H_2 evolution with a molecular 3d transition metal catalyst in pure aqueous solution was obtained, with TONs of approximately 700 for **NiP**. Advanced spectroscopic methods (TC-SPC and TAS) confirmed that directed ET from **RuP** to **NiP** occurs efficiently in all systems on the nano- to microsecond time scale. Losses due to charge recombination are minimized, as ET occurs efficiently within the lifetimes of the excited species. The highly efficient ET from dye to proton reduction catalyst is also reflected in the high photon to H_2 quantum yield of the homogeneous system of almost 10% in the presence of the sacrificial electron donor AA. Work is in progress to assemble a photoelectrode with **NiP** for use in a photoelectrochemical water splitting cell.

ASSOCIATED CONTENT

Supporting Information

Text and tables giving experimental data from kinetic and photocatalytic experiments and additional figures detailing cyclic voltammetry, kinetic measurements, and photocatalytic experiments. This material is available free of charge via the Internet at http://pubs.acs.org.

AUTHOR INFORMATION

Corresponding Author

reisner@ch.cam.ac.uk; a.reynal@imperial.ac.uk.

Notes

The authors declare no competing financial interest.

ACKNOWLEDGMENTS

The work at Cambridge was supported by the Christian Doppler Research Association (Austrian Federal Ministry of Economy, Family and Youth and National Foundation for Research, Technology and Development), the OMV Group, and the EPSRC (EP/H00338X/2). Imperial College London was supported by the ERC (project Intersolar), the Spanish Ministry of Education, and the European Commission Marie Curie CIG. This work was also supported by the "COST Action CM1202". The authors thank Dr. Xiaoe Li for assistance in TiO_2 and ZrO_2 film preparation and Ms. Bettina Basel for some help with the experimental part of the work.

REFERENCES

(1) (a) Lewis, N. S.; Nocera, D. G. *Proc. Natl. Acad. Sci. U.S.A.* **2006**, *103*, 15729−15735. (b) Youngblood, W. J.; Lee, S.-H. A.; Maeda, K.; Mallouk, T. E. *Acc. Chem. Res.* **2009**, *42*, 1966−1973. (c) Tran, P. D.; Wong, L. H.; Barber, J.; Loo, J. S. C. *Energy Environ. Sci.* **2012**, *5*, 5902−5918. (d) Wang, M.; Sun, L. *ChemSusChem* **2010**, *3*, 551−554. (e) Luo, S.-P.; Mejía, E.; Friedrich, A.; Pazidis, A.; Junge, H.; Surkus, A.-E.; Jackstell, R.; Denurra, S.; Gladiali, S.; Lochbrunner, S.; Beller, M. *Angew. Chem., Int. Ed.* **2013**, *52*, 419−423. (f) Vrubel, H.; Hu, X. *Angew. Chem., Int. Ed.* **2012**, *51*, 12703−12706. (g) Wang, X.; Xu, Q.; Li, M.; Shen, S.; Wang, X.; Wang, Y.; Feng, Z.; Shi, J.; Han, H.; Li, C. *Angew. Chem., Int. Ed.* **2012**, *51*, 13089−13092.

(2) (a) Fisher, B. J.; Eisenberg, R. *J. Am. Chem. Soc.* **1980**, *102*, 7361−7363. (b) Krishnan, C. V.; Sutin, N. *J. Am. Chem. Soc.* **1981**, *103*, 2141−2142. (c) Kellett, R. M.; Spiro, T. G. *Inorg. Chem.* **1985**, *24*, 2373−2377. (d) Hu, X.; Cossairt, B. M.; Brunschwig, B. S.; Lewis, N. S.; Peters, J. C. *Chem. Commun.* **2005**, 4723−4725. (e) Jacques, P.-A.; Artero, V.; Pecaut, J.; Fontecave, M. *Proc. Natl. Acad. Sci. U.S.A.* **2009**, *106*, 20627−20632. (f) Dempsey, J. L.; Brunschwig, B. S.; Winkler, J. R.; Gray, H. B. *Acc. Chem. Res.* **2009**, *42*, 1995−2004. (g) Artero, V.; Chavarot-Kerlidou, M.; Fontecave, M. *Angew. Chem., Int. Ed.* **2011**, *50*, 7238−7266. (h) Peuntinger, K.; Lazarides, T.; Dafnomili, D.; Charalambidis, G.; Landrou, G.; Kahnt, A.; Sabatini, R. P.; McCamant, D. W.; Gryko, D. T.; Coutsolelos, A. G.; Guldi, D. M. *J. Phys. Chem. C* **2013**, *117*, 1647−1655.

(3) (a) Na, Y.; Wang, M.; Pan, J.; Zhang, P.; Åkermark, B.; Sun, L. *Inorg. Chem.* **2008**, *47*, 2805−2810. (b) Kaur-Ghumaan, S.; Schwartz, L.; Lomoth, R.; Stein, M.; Ott, S. *Angew. Chem., Int. Ed.* **2010**, *49*, 8033−8036. (c) Streich, D.; Astuti, Y.; Orlandi, M.; Schwartz, L.; Lomoth, R.; Hammarström, L.; Ott, S. *Chem. Eur. J.* **2010**, *16*, 60−63. (d) Rose, M. J.; Gray, H. B.; Winkler, J. R. *J. Am. Chem. Soc.* **2012**, *134*, 8310−8313. (e) Li, X.; Wang, M.; Zheng, D.; Han, K.; Dong, J.; Sun, L. *Energy Environ. Sci.* **2012**, *5*, 8220−8224.

(4) (a) Collin, J. P.; Jouaiti, A.; Sauvage, J.-P. *Inorg. Chem.* **1988**, *27*, 1986−1990. (b) Wilson, A. D.; Newell, R. H.; McNevin, M. J.; Muckerman, J. T.; DuBois, M. R.; DuBois, D. L. *J. Am. Chem. Soc.* **2006**, *128*, 358−366. (c) Helm, M. L.; Stewart, M. P.; Bullock, R. M.; DuBois, M. R.; DuBois, D. L. *Science* **2011**, *333*, 863−866. (d) Yang, J. Y.; Bullock, R. M.; Shaw, W. J.; Twamley, B.; Fraze, K.; DuBois, M. R.; DuBois, D. L. *J. Am. Chem. Soc.* **2009**, *131*, 5935−5945. (e) Le Goff, A.; Artero, V.; Jousselme, B.; Tran, P. D.; Guillet, N.; Métayé, R.; Fihri, A.; Palacin, S.; Fontecave, M. *Science* **2009**, *326*, 1384−1387. (f) Zhang, W.; Hong, J.; Zheng, J.; Huang, Z.; Zhou, J.; Xu, R. *J. Am. Chem. Soc.* **2011**, *133*, 20680−20683. (g) McLaughlin, M. P.;

McCormick, T. M.; Eisenberg, R.; Holland, P. L. *Chem. Commun.* **2011**, *47*, 7989−7991. (h) Han, Z.; McNamara, W. R.; Eum, M.-S.; Holland, P. L.; Eisenberg, R. *Angew. Chem., Int. Ed.* **2012**, *51*, 1667−1670. (i) Han, Z.; Shen, L.; Brennessel, W. W.; Holland, P. L.; Eisenberg, R. *J. Am. Chem. Soc.* **2013**, *135*, 14659−14669.

(5) (a) Esposito, D. V.; Hunt, S. T.; Stottlemyer, A. L.; Dobson, K. D.; McCandless, B. E.; Birkmire, R. W.; Chen, J. G. *Angew. Chem., Int. Ed.* **2010**, *49*, 9859−9862. (b) Kirch, M.; Lehn, J.-M.; Sauvage, J.-P. *Helv. Chim. Acta* **1979**, *62*, 1345−1384.

(6) (a) Sakai, T.; Mersch, D.; Reisner, E. *Angew. Chem., Int. Ed.* **2013**, *52*, 12313−12316. (b) Reisner, E. *Eur. J. Inorg. Chem.* **2011**, 1005−1016. (c) Reisner, E.; Powell, D. J.; Cavazza, C.; Fontecilla-Camps, J. C.; Armstrong, F. A. *J. Am. Chem. Soc.* **2009**, *131*, 18457−18466. (d) Tran, P. D.; Barber, J. *Phys. Chem. Chem. Phys.* **2012**, *14*, 13772−13784. (e) Stiebritz, M. T.; Reiher, M. *Chem. Sci.* **2012**, *3*, 1739−1751. (f) Armstrong, F. A.; Hirst, J. *Proc. Natl. Acad. Sci. U.S.A.* **2011**, *108*, 14049−14054.

(7) (a) Kilgore, U. J.; Roberts, J. A. S.; Pool, D. H.; Appel, A. M.; Stewart, M. P.; DuBois, M. R.; Dougherty, W. G.; Kassel, W. S.; Bullock, R. M.; DuBois, D. L. *J. Am. Chem. Soc.* **2011**, *133*, 5861−5872. (b) Kilgore, U. J.; Stewart, M. P.; Helm, M. L.; Dougherty, W. G.; Kassel, W. S.; DuBois, M. R.; DuBois, D. L.; Bullock, R. M. *Inorg. Chem.* **2011**, *50*, 10908−10918. (c) Jain, A.; Lense, S.; Linehan, J. C.; Raugei, S.; Cho, H.; DuBois, D. L.; Shaw, W. J. *Inorg. Chem.* **2011**, *50*, 4073−4085.

(8) (a) Wilson, A. D.; Shoemaker, R. K.; Miedaner, A.; Muckerman, J. T.; DuBois, D. L.; DuBois, M. R. *Proc. Natl. Acad. Sci. U.S.A.* **2007**, *104*, 6951−6956. (b) Wiedner, E. S.; Yang, J. Y.; Chen, S.; Raugei, S.; Dougherty, W. G.; Kassel, W. S.; Helm, M. L.; Bullock, R. M.; DuBois, M. R.; DuBois, D. L. *Organometallics* **2012**, *31*, 144−156.

(9) (a) Horvath, S.; Fernandez, L. E.; Soudackov, A. V.; Hammes-Schiffer, S. *Proc. Natl. Acad. Sci. U.S.A.* **2012**, *109*, 15663−15668. (b) Small, Y. A.; DuBois, D. L.; Fujita, E.; Muckerman, J. T. *Energy Environ. Sci.* **2011**, *4*, 3008−3020.

(10) (a) Stewart, M. P.; Ho, M.-H.; Wiese, S.; Lindstrom, M. L.; Thogerson, C. E.; Raugei, S.; Bullock, R. M.; Helm, M. L. *J. Am. Chem. Soc.* **2013**, *135*, 6033−6046. (b) Tran, P. D.; Le Goff, A.; Heidkamp, J.; Jousselme, B.; Guillet, N.; Palacin, S.; Dau, H.; Fontecave, M.; Artero, V. *Angew. Chem., Int. Ed.* **2011**, *50*, 1371−1374.

(11) McKone, J. R.; Lewis, N. S.; Gray, H. B. *Chem. Mater.* **2013**, DOI: 10.1021/cm4021518.

(12) (a) Wang, F.; Wang, W.-G.; Wang, X.-J.; Wang, H.-Y.; Tung, C.-H.; Wu, L.-Z. *Angew. Chem., Int. Ed.* **2011**, *50*, 3193−3197. (b) Samuel, A. P. S.; Co, D. T.; Stern, C. L.; Wasielewski, M. R. *J. Am. Chem. Soc.* **2010**, *132*, 8813−8815. (c) Nann, T.; Ibrahim, S. K.; Woi, P.-M.; Xu, S.; Ziegler, J.; Pickett, C. J. *Angew. Chem., Int. Ed.* **2010**, *49*, 1574−1577.

(13) (a) Andreiadis, E. S.; Chavarot-Kerlidou, M.; Fontecave, M.; Artero, V. *Photochem. Photobiol.* **2011**, *87*, 946−964. (b) McNamara, W. R.; Han, Z.; Alperin, P. J.; Brennessel, W. W.; Holland, P. L.; Eisenberg, R. *J. Am. Chem. Soc.* **2011**, *133*, 15368−15371. (c) Du, P.; Schneider, J.; Luo, G.; Brennessel, W. W.; Eisenberg, R. *Inorg. Chem.* **2009**, *48*, 4952−4962. (d) Fihri, A.; Artero, V.; Razavet, M.; Baffert, C.; Leibl, W.; Fontecave, M. *Angew. Chem., Int. Ed.* **2008**, *47*, 564−567. (e) Wang, Z.-Y.; Rao, H.; Deng, M.-F.; Fan, Y.-T.; Hou, H.-W. *Phys. Chem. Chem. Phys.* **2013**, *15*, 16665−16671. (f) Lakadamyali, F.; Reynal, A.; Kato, M.; Durrant, J. R.; Reisner, E. *Chem. Eur. J.* **2012**, *18*, 15464−15475. (g) Lakadamyali, F.; Kato, M.; Muresan, N. M.; Reisner, E. *Angew. Chem., Int. Ed.* **2012**, *51*, 9381−9384. (h) Lakadamyali, F.; Kato, M.; Reisner, E. *Faraday Discuss.* **2012**, *155*, 191−205. (i) Lakadamyali, F.; Reisner, E. *Chem. Commun.* **2011**, *47*, 1695−1697. (j) Huang, J.; Mulfort, K. L.; Du, P.; Chen, L. X. *J. Am. Chem. Soc.* **2012**, *134*, 16472−16475. (k) Natali, M.; Argazzi, R.; Chiorboli, C.; Iengo, E.; Scandola, F. *Chem. Eur. J.* **2013**, *19*, 9261−9271. (l) McNamara, W. R.; Han, Z.; Yin, C.-J.; Brennessel, W. W.; Holland, P. L.; Eisenberg, R. *Proc. Natl. Acad. Sci. U.S.A.* **2012**, *109*, 15594−15599.

(14) Han, Z.; Qiu, F.; Eisenberg, R.; Holland, P. L.; Krauss, T. D. *Science* **2012**, *338*, 1321−1324.

(15) Wen, F.; Wang, X.; Huang, L.; Ma, G.; Yang, J.; Li, C. *ChemSusChem* **2012**, *5*, 849−853.

(16) Krawicz, A.; Yang, J.; Anzenberg, E.; Yano, J.; Sharp, I. D.; Moore, G. F. *J. Am. Chem. Soc.* **2013**, *135*, 11861−11868.

(17) Gardner, J. M.; Beyler, M.; Karnahl, M.; Tschierlei, S.; Ott, S.; Hammarström, L. *J. Am. Chem. Soc.* **2012**, *134*, 19322−19325.

(18) Ji, Z.; He, M.; Huang, Z.; Ozkan, U.; Wu, Y. *J. Am. Chem. Soc.* **2013**, *135*, 11696−11699.

(19) (a) Hoffert, W. A.; Roberts, J. A. S.; Bullock, R. M.; Helm, M. L. *Chem. Commun.* **2013**, *49*, 7767−7769. (b) Silver, S. C.; Niklas, J.; Du, P.; Poluektov, O. G.; Tiede, D. M.; Utschig, L. M. *J. Am. Chem. Soc.* **2013**, *135*, 13246−13249.

(20) Moore, G. F.; Sharp, I. D. *J. Phys. Chem. Lett.* **2013**, *4*, 568−572.

(21) Queffélec, C.; Petit, M.; Janvier, P.; Knight, D. A.; Bujoli, B. *Chem. Rev.* **2012**, *112*, 3777−3807.

(22) (a) Wasielewski, M. R. *Chem. Rev.* **1992**, *92*, 435−461. (b) Li, X.; Wang, M.; Zhang, S.; Pan, J.; Na, Y.; Liu, J.; Åkermark, B. r.; Sun, L. *J. Phys. Chem. B* **2008**, *112*, 8198−8202.

(23) Ito, S.; Murakami, T. N.; Comte, P.; Liska, P.; Grätzel, C.; Nazeeruddin, M. K.; Grätzel, M. *Thin Solid Films* **2008**, *516*, 4613−4619.

(24) Gillaizeau-Gauthier, I.; Odobel, F.; Alebbi, M.; Argazzi, R.; Costa, E.; Bignozzi, C. A.; Qu, P.; Meyer, G. J. *Inorg. Chem.* **2001**, *40*, 6073−6079.

(25) Fulmer, G. R.; Miller, A. J. M.; Sherden, N. H.; Gottlieb, H. E.; Nudelman, A.; Stoltz, B. M.; Bercaw, J. E.; Goldberg, K. I. *Organometallics* **2010**, *29*, 2176−2179.

(26) Bard, A. J.; Faulkner, L. R. *Electrochemical Methods: Fundamentals and Applications*, 2nd ed.; Wiley: New York, 2001.

(27) Muresan, N. M.; Willkomm, J.; Mersch, D.; Vaynzof, Y.; Reisner, E. *Angew. Chem., Int. Ed.* **2012**, *51*, 12749−12753.

(28) Espinosa, S.; Bosch, E.; Rosés, M. *Anal. Chem.* **2000**, *72*, 5193−5200.

(29) (a) Brennaman, M. K.; Patrocinio, A. O. T.; Song, W.; Jurss, J. W.; Concepcion, J. J.; Hoertz, P. G.; Traub, M. C.; Murakami Iha, N. Y.; Meyer, T. J. *ChemSusChem* **2011**, *4*, 216−227. (b) Giokas, P. G.; Miller, S. A.; Hanson, K.; Norris, M. R.; Glasson, C. R. K.; Concepcion, J. J.; Bettis, S. E.; Meyer, T. J.; Moran, A. M. *J. Phys. Chem. C* **2013**, *117*, 812−824.

(30) Borsook, H.; Keighley, G. *Proc. Natl. Acad. Sci. U.S.A.* **1933**, *19*, 875−878.

(31) Balzani, V.; Bergamini, G.; Marchioni, F.; Ceroni, P. *Coord. Chem. Rev.* **2006**, *250*, 1254−1266.

(32) Park, H.; Bae, E.; Lee, J.-J.; Park, J.; Choi, W. *J. Phys. Chem. B* **2006**, *110*, 8740−8749.

(33) (a) Xu, Y.; Schoonen, M. A. A. *Am. Mineral.* **2000**, *85*, 543−556. (b) Rothenberger, G.; Fitzmaurice, D.; Graetzel, M. *J. Phys. Chem.* **1992**, *96*, 5983−5986. (c) Bolts, J. M.; Wrighton, M. S. *J. Phys. Chem.* **1976**, *80*, 2641−2645.

(34) (a) Sayama, K.; Arakawa, H. *J. Phys. Chem.* **1993**, *97*, 531−533. (b) Lemon, B. I.; Liu, F.; Hupp, J. T. *Coord. Chem. Rev.* **2004**, *248*, 1225−1230.

(35) Macartney, D. H.; Sutin, N. *Inorg. Chim. Acta* **1983**, *74*, 221−228.

(36) (a) Brown, G. M.; Brunschwig, B. S.; Creutz, C.; Endicott, J. F.; Sutin, N. *J. Am. Chem. Soc.* **1979**, *101*, 1298−1300. (b) Sun, H.; Hoffman, M. Z. *J. Phys. Chem.* **1994**, *98*, 11719−11726.

(37) Creutz, C.; Sutin, N. *J. Am. Chem. Soc.* **1976**, *98*, 6384−6385.

(38) "On particle" ET between **RuP** and **NiP** anchored onto a colloidal suspension of ZrO_2 nanoparticles can in principle occur through an intraparticle (ET from **RuP** to **NiP** on same particle) or interparticle (ET between different particles) mechanism. Intraparticle ET is confirmed by our spectroscopic measurements, which were performed on mesoporous ZrO_2 films. Interparticle ET is not favorable because the particles are fixed within the film rather than being in a suspension. In addition, the closer proximity of **RuP** and **NiP** on the same particle favor intraparticle ET. However, a contribution from interparticle ET cannot be ruled out.

(39) Sun, Y.; Sun, J.; Long, J. R.; Yang, P.; Chang, C. J. *Chem. Sci.* **2013**, *4*, 118−124.
(40) Dong, J.; Wang, M.; Li, X.; Chen, L.; He, Y.; Sun, L. *ChemSusChem* **2012**, *5*, 2133−2138.
(41) Reynal, A.; Lakadamyali, F.; Gross, M. A.; Reisner, E.; Durrant, J. R. *Energy Environ. Sci.* **2013**, *6*, 3291−3300.
(42) Xagas, A. P.; Bernard, M. C.; Hugot-Le Goff, A.; Spyrellis, N.; Loizos, Z.; Falaras, P. *J. Photochem. Photobiol. A* **2000**, *132*, 115−120.